COVID-19 Neuropathology: Evidence for SARS-CoV-2 invasion of Human Brainstem Nuclei

Aron Emmi
University of Padova
Stefania Rizzo
University of Padova
Luisa Barzon
University of Padova
Elisa Carturan
University of Padova
Alessandro Sinigaglia
University of Padova
Silvia Riccetti
University of Padova
Mila Della Barbera
University of Padova
Rafael Boscolo Berto
University of Padova
Patrizia Cocco
University of Padova
Veronica Macchi
University of Padova
Monica De Gasperi
University of Padova
Cristina Basso
University of Padova
Raffaele De Caro (rdecaro@unipd.it)
University of Padova https://orcid.org/0000-0002-2307-0277
Andrea Porzionato
University of Padova

Article

Keywords: COVID-19, central nervous system, neuropathological alterations

Posted Date: November 15th, 2021

DOI: https://doi.org/10.21203/rs.3.rs-1055802/v1

Abstract

Neurological manifestations are common in COVID-19, the disease caused by severe acute respiratory syndrome coronavirus-2 (SARS-CoV-2). Despite some reports of detection of SARS-CoV-2 in the brain and cerebrospinal fluid of patients with COVID-19, it is still unclear whether the virus can infect the central nervous system (CNS), and which neuropathological alterations can be ascribed to viral tropism rather than immune-mediated mechanisms. Available autopsy reports are often conflictual, reporting a heterogeneous spectrum of neuropathological alterations, while viral proteins and RNA were detected only in sparse cells within the brainstem; furthermore, there appears to be no consistent correlation between viral invasion and neuropathological alterations to date.

Here, we assess the neuropathological changes occurring in 24 patients who died following a diagnosis of SARS-CoV-2 infection in Italy during the COVID-19 pandemic (from March 2020 to May 2021) and 10 age-matched controls with comparable medical conditions. Aside from a wide spectrum of neuropathological alterations, including astrogliosis, sparse lympho-monocytic infiltrations and several instances of small vessel thromboses, we identified 5 COVID-19 subjects presenting SARS-CoV-2-immunoreactive neurons within the boundaries of the solitary tract nucleus, nucleus ambiguus and substantia nigra in the brainstem. In these subjects, viral RNA was also detected by real-time RT-PCR. Quantification of reactive microglia revealed an anatomically segregated pattern of inflammation targeting mainly the medulla oblongata and the mesencephalon, and was significantly higher when compared to controls. However, SARS-CoV-2 direct invasion did not appear to correlate with the severity of neuropathological changes.

The results of this study support the neuroinvasive potential of SARS-CoV-2 by demonstrating the presence of viral proteins and genome sequences within the human brainstem, but further investigation is required to identify the link between invasion and consequent neuropathological alterations in humans.

Introduction

Neurological manifestations are common in COVID-19, the disease caused by severe acute respiratory syndrome coronavirus-2 (SARS-CoV-2)[1-5]. Symptoms range from anosmia, ageusia, dizziness and headache, which are commonly reported by patients with mild disease, to altered mental status, neuropsychiatric disorders, stroke, and, rarely, meningitis, encephalitis, and polyneuritis, which occur in hospitalized patients with severe disease[1,5]. Between 10 to 30% of people with SARS-CoV-2 infection experience long-term sequelae, referred as “long COVID”, including neurological manifestations such as hyposmia, hypogeusia, headaches, fatigue, sleep disorders, pain, and cognitive impairment[3]. Despite some reports of detection of SARS-CoV-2 in the brain and cerebrospinal fluid of patients with COVID-19[2-3,6], it is still unclear whether the virus can infect the central nervous system (CNS). In particular, it still remains to be elucidated whether neurological manifestations and neural damage are a direct consequence of viral invasion of the CNS, are due to post-infectious immune-mediated disease, or are the result of systemic disease[1,6-11]. Studies on human neural cell cultures and brain organoids report conflicting data on SARS-CoV-2 neurotropism[12]. Overall, they suggest that SARS-CoV-2 does not infect and replicate efficiently in human neural cells, while it can replicate at high rates in choroid plexus epithelial cells[7,13-14]. At variance, intranasal inoculation of SARS-CoV-2 in transgenic mice overexpressing human ACE2 under the K18 promoter resulted in brain invasion and widespread infection of neurons, radial glia and neuronal progenitor cells[15-16]. Other coronaviruses, such as SARS-CoV and MERS-CoV, appear to be able to infect the CNS in both humans and animal models[17].

Data deriving from large autopsy studies in patients who died from COVID-19 suggest for the neuroinvasive potential of SARS-CoV-2 in the CNS[8-9,17], even though infection appears to be limited to sparse cells in the brainstem and not associated with encephalitis or other specific changes referable to the virus[8]. However, other studies failed to detect SARS-CoV-2 antigens or genomic sequences in brain tissues of COVID-19 patients[11,17-18]. Neuropathological changes in the brain of COVID-19 patients are mild and mainly represented by ischaemic lesions, astrogliosis, microglial nodules, and cytotoxic T lymphocyte infiltrates, most pronounced in the brainstem, cerebellum, and meninges[8-9,11,18,21]. Deep spatial profiling of the local immune response in COVID-19 brains through imaging mass spectrometry revealed significant immune activation in the CNS with pronounced neuropathological changes (astrocytosis, axonal damage, and blood-brain-barrier leakage) and detected viral antigen in ACE2-positive cells enriched in the vascular compartment[18]. Microglial nodules and the perivascular compartment represented COVID-19-specific, microanatomic-immune niches[18]. Single-nucleus gene-expression profiling of frontal cortex and choroid plexus tissues from severe COVID-19 patients showed broad perturbations with upregulation of genes involved in innate antiviral response and inflammation, microglia activation and neurodegeneration[20]. As evidenced by the above case series, and considering the different case reports available[22-24], SARS-CoV-2 infection of CNS seems to be limited to isolated cells within the brainstem and cranial nerve axons of the lower medulla and have been reported in few cases of the various autopsy series, while widespread neuropathological sequelae (such as astrogliosis, microgliosis, lymphocyte infiltration, microvascular injury, fibrinogen leakage) have been documented in most examined specimen.

In the preset study, we assess the neuropathological changes of 24 patients who died following a diagnosis of SARS-CoV-2 infection in Italy during the COVID-19 pandemic (from March 2020 to May 2021) and 10 age-matched controls with comparable medical conditions.

Study design and Materials

Hospitalized patients who died following a diagnosis of SARS-CoV-2 infection in the Veneto Region, Italy, during the peak incidence of COVID-19 (from March 2020 to May 2021) were autopsied according to established COVID-19 infection security protocols. Inclusion criteria for the study were: a) diagnosis of SARS-CoV-2 infection confirmed by molecular testing of naso-pharyngeal swabs and b) high-quality brain tissue samples available for histopathological and immunohistochemical analysis. A total of 24 patients were included in the study.

10 age-matched control cases with similar general medical conditions, predating the COVID-19 pandemic in Italy, were included to compare for activated microglial density in the brainstem while also serving as controls for viral protein immunohistochemical staining.

Methods

Sampled brains were fixed in 4% phosphate-buffered formalin solution following autopsy and subsequently sectioned for histopathological and immunohistochemical analysis. Samples of the cerebral cortex, basal ganglia, hippocampus, cerebellar cortex, deep cerebellar nuclei, choroid plexuses and meninges were obtained, while the brainstem was isolated at the level of the rostral extremity of the mesencephalon and extensively sampled in its whole cranio-caudal extent. The 12 cranial nerves, where available, including the olfactory bulb, tract and bifurcation, were also sampled.

Haematoxylin and eosin stain was employed for histopathological evaluation. Immunoperoxidase staining was performed on a Dako EnVision Autostainer (Dako Denmark A/S, Glostrup, Denmark) according to manifacturer recommendations. Antibodies for CD3 (Polyclonal Rabbit Anti-Human, Dako Omnis, Code Number: GA503), CD20 (Monoclonal Mouse Anti-Human, Clone KP1, Dako Omnis, Code Number: M0814) and CD68 (Monoclonal Mouse Anti-Human, Clone L26, Dako Omnis, Code Number: M0756) were employed to characterize lympho-monocytic infiltrations. Microglial Activation was assessed using both CD68 (as above) and HLA-DR Antibodies (Monoclonal Rabbit Anti-Human, Clone: LN-3, Invitrogen, Thermo Fisher Scientific, Waltham, MA, USA). Anti-GFAP immunohistochemistry (Polyclonal Rabbit Anti-Human, DAKO Omnis, Code Number: GA524) was employed to assess reactive astrogliosis. Anti-CD61 immunohistochemistry (Monoclonal Mouse Anti-Human, Clone Y2/51, Dako Omnis, Code Number: M0753) was also employed to evaluate the presence of platelet microthrombi.

Anti-SARS-CoV-2 nucleocapsid (Rabbit Anti-Human, Sino Biologicals, 40143-R001) and -Spike Subunit 1 Antibody (Monoclonal Rabbit Anti-Human, Clone 007, Sino Biological, Code Number: 40150-R007) immunostainings were employed to evaluate viral tropism within the tissue. The expression of ACE2 Receptor protein (Rabbit Anti-Human Polyclonal, Abcam, Code Number: ab15348) and TMPRSS-2 protein (Rabbit Anti-Human Monoclonal, Abcam, Code Number: ab242384) was assessed within the brainstem and cerebellum, and in all sections with positive findings for viral proteins.

Anti-nucleocapsid and anti-spike antibodies were validated through SARS-CoV-2 infected Vero E6 cells and autopsy-derived lung tissue from SARS-CoV-2 infected patients as positive controls; non-infected cells and lung sections deriving from autopsy cases predating COVID-19 pandemic (2017) were used as negative controls (Supplementary Figure 1). Peroxidase reactions were repeated at least three times to ensure reaction consistency.

Real-time RT-PCR analyses were performed to detect SARS-CoV-2 genome sequences. Briefly, total RNA was purified from this selected material using a RecoverAll™ Total Nucleic Acid Isolation kit (Thermo Fisher Scientific) following the manufacturer's instructions. One-step real-time RT-PCR assays targeting SARS-CoV-2 nucleocapsid (N) coding region were run on ABI 7900HT Sequence Detection Systems (Thermo Fisher Scientific), as previously reported[25].

Slides were examined by experienced neuropathologists and morphologists blind to patient clinical findings. Disagreements were resolved by consensus. The degree of astrogliosis and microgial proliferation was classified using a four-tiered semi-quantitative approach for each evaluated section, while microglial activation was quantified by the means of digitally-assisted immunoreactivity quantification by experienced morphometrists.

Quantification of Activated Microglia

The degree of microgliosis was assessed through a digitally-assisted quantification approach at the level of the medulla, pons and mesencephalon. For each subject, standard sections passing through the area postrema (medulla), facial colliculus (pons) and red nucleus (midbrain) were processed for HLA-DR immunoperoxidase staining. Photomicrographs were acquired under a Leica DM4500B microscope (Leica Microsystems) connected to a Leica DFC320 high-resolution digital camera (Leica Microsystems) and a computer equipped with softwares for image acquisition (QWin, Leica Microsystems) and analysis (ImageJ). Immunoreactivies were evaluated according to morphology and counted manually within six counting fields (fields of view, FOV) spanning across the dorsal-to-ventral axis of the sections; FOV structures and boundaries are summarized in Supplementary Table 1 for each level of sectioning. The number of immunoreactivites per mm^2 was

calculated for each counting field and assigned to one anatomical compartment (i.e. tegmentum, tectum and basis), based on their topography according to Mai and Paxinos[26]. Comparisons and statistical evaluations were conducted per individual FOV, anatomical compartment and level of section (medulla, pons, mesencephalon).

Statistical Analyses

Statistical analyses and visualizations were performed using GraphPad Prism 9. Differences in activated microglia counts (microglia / mm^2) between COVID-19 and control patients in Figures 2B, 3B and 4B, were analyzed by t tests with Welch's correction. Microglial density in the different FOV in Figures 2C, 3C, and 4C were determined by ordinary one-way ANOVA tests for each level of sectioning. Tukey multiple comparisons test was performed. Further statistical details for each plot can be found in the corresponding figure legend. Throughout the manuscript * indicates $p < 0.05$, ** $p < 0.01$, *** $p < 0.001$ and **** $p < 0.0001$.

Results

Clinical Data

Twenty-four COVID-19 patients were included in the study. In all patients, SARS-CoV-2 RNA was detected by molecular testing in naso-pharyngeal swabs. Eleven were females, while 13 were males. The mean age of the included subjects was 73±13.7 years. Most included subjects were affected by preexisting chronic medical conditions, such as hypertension (N=13, 7 females, 6 males). Eleven patients (7 female, 4 male) were affected by neurological or neurodegenerative disease prior to SARS-CoV-2 infection. Twenty-three patients were hospitalized prior to death. Patients were hospitalized for 14.5±11.3 days and died 1 to 34 days following admission. The available clinical data for our cohort is reported in Table 1.

Ten age-matched control subjects were included in the study. All patients were negative for SARS-CoV-2 infection or died prior to the COVID-19 pandemic in Italy. Two were female, while 8 were male. The mean age of included controls was 74±14 years. All patients presented chronic medical conditions including hypertension, diabetes, and hypercolesterolemia. Three patients died due to pneumonia. Three patients had a clinical diagnosis of dementia. The available clinical data for the control group are reported in Table 2.

Neuropathological examination

The brains of 20 COVID-19 subjects displayed gross macroscopic abnormalities including mild-to-moderate cerebral atrophy (N=9), moderate edema (N=9), territorial ischemic injury (n=6) and severe pontine atrophy (N=1).

Histopathological evaluation revealed haemorragic injury in four patients and small vessel thromboses in nine patients; thromboses were identified mainly at the level of the pons, deep cerebellar nuclei and cerebral cortex, with one patient presenting thromboses in multiple sites. Enlarged perivascular and perineuronal spaces, indicative of mild to moderate edema, were present in 22 subjects and were more pronounced at the level of the brainstem and basal ganglia, with particular regard to the medullary tegmentum. Small vessels were congested in most subjects with moderate perivascular extravasation at the level of the medulla, pons and deep cerebellar nuclei in six cases. Fresh territorial ischaemic injuries were evident in five patients. Old territorial ischaemic lesions were found in six subjects.

Variable degrees of astrogliosis were evident in all subjects in all assessed regions, but were more pronounced at the level of the medullary tegmentum, pons and substantia nigra (Figure 2). Reactive Bergmann Glia was found in the cerebellar cortex of 5 patients; for the detailed assessment of astrogliosis within sampled regions, refer to Table 3.

Parenchymal and perivascular microglia appeared activated and with increased phagocytic activity, as testified by HLA-DR / CD68+ immunoreactivity, in 23 assessed subjects, with particular involvement of the brainstem and basal ganglia. Moderate to severe perivascular CD68+ macrophage infiltration was found in 23 subjects, while parenchymal macrophages were particularly evident at the level of the substantia nigra of 12 subjects. Microglial stars associated with perineuronal CD68+ and HLA-DR+ cells were suggestive of neuronophagia in 18 subjects and were identified at the level of the substantia nigra (N=14), dorsal motor nucleus of the vagus (N=12), medullary reticular formation (N=9), area postrema (N=6) and basal ganglia (N=5).

Microgliosis: Quantification and Distribution of Activated Microglia

Microgliosis was more pronounced within the medulla, pons and brainstem in COVID-19 patients and statistically significant differences ($p<0.001$; $p<0.001$; and $p<0.0001$, respectively) were found when compared to age-matched controls, as seen in Welch's corrected T-test plots in Figure 3B, 4B, 5B. The topographical distribution of activated microglial cells within the anatomical boundaries of the brainstem and its nuclei can be appreciated in Figure 3A, 4A and 5A.

At the level of the medulla of COVID-19 patients, single-way ANOVA of individual FOVs (Figure 2C) revealed statistically significant differences ($p<0.001$) between FOVs located within the boundaries of the tegmentum, when compared to FOVs of the Medullary Pes; no differences were found between FOVs located within the same anatomical compartment. At the level of the Pons, no significant differences in activated microglial density were found between FOVs or anatomical compartments (Figure 3C).

In the Mesencephalon, statistically significant differences were found when comparing FOVs of the Tegmentum (FOV1, FOV2) to FOVs of the Tectum (FOV3,FOV4) and Pes (FOV5,FOV6) as seen in Figure 4C. Furthermore, statistically significant differences were found between FOV3 and FOV4, with the latter displaying higher activated microglial counts ($p<0.001$), suggesting an increasing dorsal-to-ventral gradient of microgliosis within the structure.

SARS-CoV-2 Tropism

Immunoperoxidase staining for SARS-CoV-2 spike protein (Spike Subunit 1) and nucleocapsid protein was performed on all samples of included subjects and controls and showed positive results in cases with SARS-CoV-2 infection, but not in controls. In particular, viral proteins were detected in four subjects (#1-4) at the level of the cerebellar meninges, in seven subjects (#3, #7, #9, #10, #11, #17, #18) within CNS parenchima, in five subjects (#3, #7, #9, #10, #17) with immunoreactive neurons within the anatomically defined boundaries of the solitary tract nucleus, nucleus ambiguus and substantia nigra. Some of these subjects (#7, #11, #17, #18) also displayed endothelial cell immunoreactivity in small vessels of the cerebral cortex (subject #11), deep cerebellar nuclei (#17-18) and hippocampus (#7) (Supplementary Figure 2); small vessel thromboses, perivascular extravasation and haemorragic injury were found within affected regions of these cases.
In case #7, ischaemic injury of the right rostral hippocampal formation due PCA occlusion was associated to perivascular extravasation, oedema, fibrinogen leakage and viral protein immunoreactivity within small vessel endothelium, further confirmed by RT-PCR. Haemorragic injury in the territory of the right MCA in #11 was associated to marked endothelitis within perilesional tissue, presenting both viral protein immunoreactive endothelium and positive RT-PCR. Similarly, the deep cerebellar white matter and dentate nuclei in cases #17-18 presented small vessel thromboses and extensive haemorragic injury. Conversely, in some cases with small vessel thromboses within the pons and frontal cortex (e.g. #19-20), viral proteins and RNA was not detectable. The distribution and topography of SARS-CoV-2 protein immunoreactivities is summarized in Figure 6A-D. Histopathological evaluation for each subject and in each assessed region is reported in Table 3.

Molecular testing by real-time RT-PCR detected SARS-CoV-2 RNA in 10 out of 24 COVID-19 subjects, 9 of whom had also SARS-CoV-2 S and/or N protein-positive IHC (Table 3). In positive tissue samples, threshold cycles (Ct) of real-time RT-PCR for SARS-CoV-2 RNA ranged between 33 and 38, while in all samples the Ct values of the internal control RNAseP ranged between 27 and 34.

ACE2 receptor protein and TMPRSS2 protein immunoreactivity was compatible with the anatomical distribution of SARS-CoV-2 proteins (Supplementary Figure 1, E-F). Both proteins were expressed in the endothelial cells of small vessels within the medulla oblongata, pons and mesencephalon, and mild immunoreactivity was also detected in morphologically-identifiable neurons and oligodendroglial cells within the vagal trigone, nucleus ambiguus and substantia nigra.

Discussion

In the present study, the neuropathological findings of 24 COVID-19 patients were examined and compared with age matched-controls with comparable medical conditions. Our findings indicate, in line with some of the previous autopsy reports, specific neuropathological alterations in the brains of COVID-19 patients, with particular regard to topographically-defined microgliosis within anatomical compartments of the brainstem and viral immunoreactivity in specific loci of the CNS, either within the boundaries of brainstem nuclei or in the context of ischaemic and haemorragic injuries. Platelet and fibrin microthrombi, in particular, were characteristic findings of the COVID-19 cohort, and often affected multiple organs, such as the lungs, liver, intestine, and hypopharynx and even the carotid body[10,27–28], as summarized in Table 1. Microthromboses were more frequent within the pons, deep cerebellar nuclei and cerebral cortex. In some cases, haemorragic injury and microthromboses were found in regions with viral protein immunoreactivity in vascular endothelial cells.

SARS-CoV-2 neuronal tropism, on the other hand, was confined to specific loci of the CNS. As seen in Figure 6A-D, SARS-CoV-2 appears to be localized preferentially within neurons of the vagal nuclei of the medulla and the substantia nigra of the mesencephalon, with the exception of one subject who also presented immunoreactive cells throughout the whole brainstem. While Matschke et al.[8] reported SARS-CoV-2 invasion of cranial nerves IX-X, we were unable to replicate these findings within our cohort; furthermore, unlike Meinhardt et al's findings[9], viral proteins and RNA were not detectable in any of the sampled olfactory bulbs, tracts and bifurcations, even though moderate oedema, moderate-to-severe astrogliosis and moderate microglial activation was encountered in most cases. ACE2 Receptor and TMPRSS-2 protein immunohistochemistry support this topographical localization, with neurons within the Dorsal Motor Nucleus of the Vagus, Solitary Tract Nucleus, Nucleus Ambiguus and Substantia Nigra being moderately immunoreactive (Supplementary Figure 1, E-F).

While previous studies identified viral protein immunoreactivity in sparse cells throughout the brainstem[8–18], our findings appear to be in line with available animal studies on other coronaviruses, i.e. SARS-CoV and MERS-CoV, which are known to be able to infect the brainstem, and particularly the solitary tract nucleus and nucleus ambiguus, so that an analog pattern of neuroinvasion for SARS-CoV-2 has been suggested[17,29–31]. Internalization of SARS-CoV-2 is known to cause inhibition of ACE-2 activity and progressive depletion of membrane-bound ACE-2[30–31], with subsequent ACE1/ACE2 imbalance and increase in Angiotensin II (AngII). Circulating AngII may in turn increase the sympathetic output both centrally, at the level of the circumventricular organs (area postrema and subfornical organ)[32], and peripherally, by acting on the carotid body[10,30–32]. As ACE-2 is also expressed in the solitary tract nucleus, sympathetic activation may be furtherly increased by local ACE1/ACE2 imbalance and AngII stimulation. Thus, COVID-19-induced increase in AngII may represent an additional way to furtherly worsen sympathoactivation, which may exert significant detrimental effect through its actions on lungs, heart, vessels, kidney, metabolism, and/or immune system, representing a so-far undervalued mechanism at the basis of the vicious circle between COVID-19 and known comorbidities[30–31].

However, while the hypothesized effects of SARS-CoV-2 invasion of the CNS remain to be investigated, post-mortem evidence of direct viral invasion in humans, with analog topographical distribution to animal models, represents a relevant step towards the elucidation of COVID-19 pathophysiology.

As for HLA-DR reactive activated microglia, we found significant differences between COVID-19 patients and controls in all assessed levels of the brainstem, however the COVID-19 group was also characterized by higher density of activated microglia within specific anatomical loci, such as the medullary and mesencephalic tegmentum. Our findings appear to be in line with Schwabenland et al.[18], who identified microglial nodules and perivascular HLA-DR+ reactive microglia as hallmark for COVID-19, in contrast to both controls and ExtraCorporeal Membrane Oxygenation (ECMO) patients. Conversely, Deigendesh et al.[33] found significant differences in HLA-DR+ activated microglia when comparing COVID-19 subjects to non-septic controls, but no differences were found with patients who had died under septic conditions; according to Deigendesh et al.[33] this may represent a histopathological correlate of critical illness-related encephalopathy, rather than a COVID-19-specific finding. In our study, the evidenced pattern of microgliosis appears to match with the distribution of SARS-CoV-2 immunoreactivities, localized mainly within the vagal complex and the substantia nigra. However, when comparing COVID-19 patients with and without viral immunoreactivity, no statistically significant differences in the overall degree of brainstem microgliosis were found, as seen in Figure 5. Hence, microglial activation does not appear to be directly related to neuronal invasion of SARS-CoV-2 within affected regions, but could represent the consequence of systemic infection / cytokine storm ongoing during COVID-19 affecting topographic compartments of the brainstem with an intrinsic anatomical vulnerability, such as the medullary tegmentum, and the substantia nigra[34–35]. Furthermore, COVID-19 is characterized by different evolutionary phases and heterogeneous individual responses, and the short interval between infection and death in our cohort (mean hospitalization time = 14 days) and the fact that included patients died during the acute phase of the disease, may not be sufficient to determine detectable neuropathological alterations as a direct consequence of viral invasion, which may require more time to develop[3,31]. In this perspective, future studies on “long COVID” patients[3] may be able to shed a light on the long-term consequences of COVID-19, particularly concerning the detection of SARS-CoV-2 within the CNS after the acute phase of the disease, and whether or not this leads to specific neuropathological alterations as a consequence of viral invasion.

Conclusions

The present study contributes to define the spectrum of neuropathological alterations in COVID-19, as well as the neuroinvasive potential of SARS-CoV-2 within the CNS. Unlike previous findings, we have documented several cases in which viral proteins and RNA were clearly detectable within anatomically defined regions of the CNS. Similarly, microglial activation in the brainstem seems to be significantly different between COVID-19 and controls, with the former also presenting a pattern of increased microglial density in specific compartments of the medulla and midbrain.
In line with available literature, however, SARS-CoV-2 direct invasion does not appear to directly correlate with the severity of neuropathological changes, such as microglial activation. Hence, the spectrum of neuropathological alterations described could be ascribed to systemic infection, rather than direct viral invasion, and require further confirmation from other studies.

Declarations

Data Sharing: data is available from the corresponding author upon request.

Conflicts of interest: the authors declare no conflicts of interest.

Ethical approval: All procedures were carried out in accordance to the Declaration of Helsinki. Samples were anonymous to the investigators and used in accordance with the directives of the Committee of the Ministers of EU member states on the use of samples of human origin for research.

Tables

TABLE 1. Clinical data and autoptic findings of the COVID-19 cohort.

Case	Age	Sex	Hospitalization (days)	Hypertension	Antemortem Head CT	Neurological signs	Microthrombosis (NON-CNS)	Autoptic Findings
#1	87	F	2	Y	NA	Cognitive decline	Lungs, liver	Diffuse alveolar damage
#2	92	F	5	N	NA	Cognitive decline, Alzheimer type	Lungs	Diffuse aveolar damage, intestinal infarction
#3	83	M	8	Y	Cerebral and cerebellar atrophy, chronic ischemic vascular disease	Previous ischaemic insult in the left frontoparietal area with right hemiparesis; episodes of hepatic encephalopathy (HCV+)	No	Diffuse alveolar damage, hepatic cyrrhosis
#4	97	F	9	Y	NA	Vascular dementia	Lungs	Diffuse alveolar damage, cardiac amyloidosis
#5	78	F	15	Y	NA	NA	Liver	Pneumopathia, aspergillus bronchopneumonia
#6	74	M	13	Y	Vascular calcification, expansive lesion of the right frontal lobe and right cerebellar hemisphere in patient with pulmonary neoplasia	NA	No	Small cell metastatic lung carcinoma, diffuse alveolar damage
#7	58	F	11	N	Extensive ischaemic lesion of the territory of the right PCA, occulsion of the PCA	NA	No	Acute myocardial infarction, cardiogenic shock
#8	50	M	1	N	NA	NA	No	Coronary atherosclerosis and myocardiosclerosis
#9	81	F	30	Y	Ischaemic regions in the MCA territory and diffuse cerebral and cerebellar atrophy due to chronic vascular ischaemic disease.	Soporous status	Lungs, liver	Atherosclerotic aortic aneurysm, pneumopathia.
#10	60	M	30	N	NA	NA	Heart	Pneumopathia with emphysema.
#11	55	M	15	N	NA	NA	No	Pulmonary thromboembolism with infarcts.
#12	62	M	27	N	NA	NA	Lungs	Pneumopathia with hemorrhages. Intestinal and hepatic infarcts.
#13	73	M	21	Y	NA	NA	No	Right pleurodesis.

#14	58	F	24	Y	Right anisocoria	No relevant signs	Lungs	Pneumopathia. Necrotic-haemorragic pancreatitis. Multiorgan failure.
#15	49	F	3	N	Confusion and hallucinations; CSF Streptococcus Pneumoniae +	NA	No	Acute purulent meningitis. Post-anoxic cerebral death.
#16	72	M	10	Y	Hypostenia, dizziness, anosmia. Sudden fall.	NA	No	Consolidative pneumopathia. Hypertensive heart disease.
#17	72	M	38	N	NA	NA	No	Multivascular obstructive coronary atherosclerosis. Left pulmonary infarct.
#18	82	M	6	Y	Acute neurological event: Anisocoria, non responding	NA	No	Lobar pneumonia
#19		F	1	Y	NA	NA	NA	
#20		M	NA	Y	NA	NA	NA	
#21	73	M	5	N	NA	NA	Lungs	Diffuse alveolar damage, Platelet/fibrin microthrombosis
#22	77	F	34	Y	No signs	NA	Lungs	Chronic emphysema, diffuse alveolar damage and platelet/fibrin microthromboses.
#23	84	M	12	Y	Chronic ischaemic vascular disease	Cognitive decline Parkinson's Disease Prior aneurysm rupture and hemorrhagic stroke	Lungs	Chronic emphysema, bacterial pneumonia, diffuse alveolar damage lung platelet/fibrin microthrombosis.
#24	89	F	1 (died in a retirement home)	Y	Chronic ischaemic vascular disease, territorial ischaemic injury (right occipital lobe, caudate nucleus and cerebellum)	Dementia (NS)	Lungs	Chronic emphysema, diffuse alveolar damage and platelet/fibrin microthromboses

TABLE 2. Clinical and anagraphic data of the control cohort.

ID	SEX	AGE	HYPERTENSION	AUTOPTIC FINDINGS / CAUSE OF DEATH
CTRL1	F	79	Y, diabetes, hypercol.	Pentalobar pneumonia, Respiratory Insufficiency.
CTRL2	M	75	Y	Bronchopneumonia, subdural haematoma.
CTRL3	M	40	N	Haemorragic Shock.
CTRL4	M	74	Y	Cardiac arrest, prior infarction.
CTRL5	M	76	Y, hypercolest.	Cardiac arrest, prior deep venous thrombosis
CTRL6	M	90	Y, hypercolest.	Head trauma, Cardiac Arrest
CTRL7	M	83	Y, renal insuff.	Ischaemic heart disease, Cardiac Arrest
CTRL8	M	85	Y, diabetes	Natural death; dementia ns
CTRL9	M	62	NS	Bacterial endocarditis, aortic valve insufficiency, fronto-parietal ischaemia.
CTRL10	F	78	N	Pneumonia, cardiac arrest.

TABLE 3. Histopathological and Immunohistochemical findings in the COVID-19 Subjects. N and S indicate the viral antigen detected in the tissue. N, Nucleocapsid Protein; S, Spike Protein; RT-CT, Real Time Cycle.

	Mild
	Moderate
	Severe
	Absent / Negative
	Present / Positive

CASE	SAMPLE / LEVEL	ASTROGLIOSIS (GFAP)	MICROGLIOSIS (CD68 – HLA-DR)	THROMBOSES / SMALL VESSEL THROMBOSES (H&E – CD61)	VIRAL PROTEINS (IHC)	VIRAL RNA (RT-PCR)
#1	Medulla Oblongata		191.6 Microglia / mm^2			
	Pons		141.5 Microglia / mm^2			
	Midbrain		169.8 Microglia / mm^2			
	Cerebellar Cortex					
	Basal Ganglia					
	Frontal Cortex					
	Olfactory bulbs and tracts					
	Cranial Nerves (III-XI)					
	Leptomeninges				S	
	Choroid Plexuses					
#2	Medulla Oblongata		167.6 Microglia / mm^2			
	Pons		124.5 Microglia / mm^2			
	Midbrain		183.5 Microglia / mm^2			
	Cerebellar Cortex					
	Basal Ganglia					
	Frontal Cortex					
	Olfactory bulbs and tracts					
	Cranial Nerves (III-XI)					
	Leptomeninges				S	
	Choroid Plexuses					
#3	Medulla Oblongata		304 Microglia / mm^2		S, N	
	Pons		288 Microglia / mm^2		S, N	
	Midbrain		218 Microglia / mm^2		S, N	
	Cerebellar cortex					
	Basal Ganglia				S	
	Frontal Cortex					

	Olfactory bulbs and tracts					
	Cranial Nerves (III-XI)					
	Leptomeninges				S	
	Choroid Plexuses					
#4	Medulla Oblongata		174.8 Microglia / mm^2			
	Pons		133.6 Microglia / mm^2			
	Midbrain		183.5 Microglia / mm^2			
	Cerebellar Cortex					
	Basal Ganglia					
	Frontal Cortex					
	Olfactory bulbs and tracts					
	Leptomeninges				S	
	Choroid Plexuses					
#5	Medulla Oblongata		158.8 Microglia / mm^2			
	Pons		128.8 Microglia / mm^2			
	Midbrain		156.5 Microglia / mm^2			
	Cerebellar Cortex					
	Deep cerebellar nuclei					
	Basal Ganglia					
	Hippocampus					
	Frontal Cortex					
	Olfactory bulbs and tracts					
	Leptomeninges					
	Choroid Plexuses					
#6	Medulla Oblongata		106.2 Microglia / mm^2			
	Pons		129.3 Microglia / mm^2			
	Midbrain		114.3 Microglia / mm^2			
	Cerebellar Cortex					
	Deep cerebellar nuclei					
	Basal Ganglia					
	Hippocampus					

	Frontal Cortex					
	Leptomeninges					
	Choroid Plexuses					
#7	Medulla Oblongata		184.2 Microglia / mm^2		S	RT-CT=35,46
	Pons		129.3 Microglia / mm^2			
	Midbrain		157.5 Microglia / mm^2		S	RT-CT=39,96
	Cerebellar Cortex					
	Deep cerebellar nuclei					
	Basal Ganglia					
	Hippocampus				S, N	RT-CT=38,04
	Frontal Cortex					
	Leptomeninges					
	Choroid Plexuses					
#8	Medulla Oblongata		84.8 Microglia / mm^2			
	Pons		89.1 Microglia / mm^2			
	Midbrain		97.6 Microglia / mm^2			
	Cerebellar Cortex					
	Deep cerebellar nuclei					
	Basal Ganglia					
	Hippocampus					
	Frontal Cortex					
	Leptomeninges					
	Choroid Plexuses					
#9	Medulla Oblongata		277.2 Microglia / mm^2		S, N	RT-CT=37,4
	Pons		176.8 Microglia / mm^2			
	Midbrain		204.6 Microglia / mm^2		N	RT-CT=38,14
	Cerebellar Cortex					
	Deep cerebellar nuclei					
	Basal Ganglia					
	Hippocampus					
	Frontal Cortex					
	Leptomeninges				S	RT-

						CT=37,4
	Choroid Plexuses					
#10	Medulla Oblongata		240 Microglia / mm^2		N	ND
	Pons		164.3 Microglia / mm^2			
	Midbrain		224 Microglia / mm^2		N	ND
	Cerebellar Cortex					
	Deep cerebellar nuclei					
	Basal Ganglia					
	Frontal Cortex and subcortex				S, N	RT-CT=37,61
	Leptomeninges					
	Choroid Plexuses					
#11	Medulla Oblongata		208.8 Microglia / mm^2			
	Pons		130.1 Microglia / mm^2			
	Midbrain		172.8 Microglia / mm^2			
	Cerebellar Cortex					
	Deep cerebellar nuclei					
	Basal Ganglia					
	Frontal Cortex					
	Parietal Cortex				S S	RT-CT=38,00
	Leptomeninges					
	Choroid Plexuses					
#12	Medulla Oblongata		190.4 Microglia / mm^2			
	Pons		119.1 Microglia / mm^2			
	Midbrain		173.6 Microglia / mm^2			
	Cerebellar Cortex					
	Deep cerebellar nuclei					
	Basal Ganglia					
	Frontal Cortex					
	Leptomeninges					
	Choroid Plexuses					
#13	Medulla Oblongata		275.2 Microglia / mm^2			

	Pons		**195.8 Microglia / mm^2**			
	Midbrain		**205.5 Microglia / mm^2**			
	Cerebellar Cortex					
	Deep cerebellar nuclei					
	Basal Ganglia					
	Frontal Cortex					
	Leptomeninges					
	Choroid Plexuses					
#14	Medulla Oblongata		**161.4 Microglia / mm^2**			
	Pons		**114.8 Microglia / mm^2**			
	Midbrain		**130.6 Microglia / mm^2**			
	Cerebellar Cortex					
	Deep cerebellar nuclei					
	Basal Ganglia					
	Frontal Cortex					
	Leptomeninges					
	Choroid Plexuses					
#15* Poor tissue quality	Medulla Oblongata					
	Pons					
	Midbrain					
	Deep cerebellar nuclei					
	Basal Ganglia					
	Frontal Cortex					
	Leptomeninges					
	Choroid Plexuses					
#16	Medulla Oblongata		**225.6 Microglia / mm^2**			
	Pons		**128.8 Microglia / mm^2**			
	Midbrain		**184.5 Microglia / mm^2**			
	Cerebellar Cortex					
	Deep cerebellar nuclei					
	Basal Ganglia					RT-CT=37,47

	Frontal Cortex					
	Leptomeninges					
	Choroid Plexuses					
#17	Medulla Oblongata		191.8 Microglia / mm^2		S	RT-CT=38,34
	Pons		142.8 Microglia / mm^2			
	Midbrain		149.8 Microglia / mm^2		N	ND
	Cerebellar Cortex					
	Deep cerebellar nuclei				S, N	ND
	Basal Ganglia					
	Frontal Cortex					
	Leptomeninges					
	Choroid Plexuses					
#18	Medulla Oblongata		182.8 Microglia / mm^2			
	Pons		139.6 Microglia / mm^2			
	Midbrain		149.8 Microglia / mm^2			
	Cerebellar Cortex					
	Deep cerebellar nuclei				S	RT-CT=37,33
	Basal Ganglia					
	Frontal Cortex					
	Leptomeninges					
	Choroid Plexuses					
#19	Pons		211 Microglia / mm^2			
	Midbrain		156.1 Microglia / mm^2			
	Cerebellar Cortex					
	Deep cerebellar nuclei					
	Basal Ganglia					
	Occipital Cortex					
	Frontal Cortex					
	Parietal Cortex					
	Temporal Cortex					
#20	Pons		162.6 Microglia / mm^2			
	Midbrain		158.5 Microglia / mm^2			

	Cerebellar Cortex					
	Deep cerebellar nuclei					
	Basal Ganglia					
	Occipital Cortex					
	Frontal Cortex					
	Parietal Cortex					
	Temporal Cortex					
#21	Medulla Oblongata		107 Microglia / mm^2			
	Pons		112.1 Microglia / mm^2			
	Midbrain		117.5 Microglia / mm^2			
	Cerebellar Cortex					
	Deep cerebellar nuclei					
	Basal Ganglia					
	Hippocampus					
	Frontal Cortex					
	Parietal Cortex					
	Temporal Cortex					
	Leptomeninges					
	Choroid Plexuses					
#22	Medulla Oblongata		219.1 Microglia / mm^2			
	Pons		155 Microglia / mm^2			
	Midbrain		173.6 Microglia / mm^2			
	Cerebellar Cortex					
	Deep cerebellar nuclei					
	Basal Ganglia					
	Hippocampus					
	Frontal Cortex					
	Parietal Cortex					
	Temporal Cortex					
	Leptomeninges					
	Choroid Plexuses					
#23	Medulla Oblongata		170.3 Microglia / mm^2			

	Pons		167.6 Microglia / mm^2			
	Midbrain		205.6 Microglia / mm^2			
	Cerebellar Cortex					
	Deep cerebellar nuclei					
	Basal Ganglia					
	Hippocampus					
	Frontal Cortex					
	Parietal Cortex					
	Temporal Cortex					
	Leptomeninges					
	Choroid Plexuses					
#24	Medulla Oblongata		178.1 Microglia / mm^2			
	Pons		157.1 Microglia / mm^2			
	Midbrain		172.8 Microglia / mm^2			
	Cerebellar Cortex					
	Deep cerebellar nuclei					
	Basal Ganglia					
	Hippocampus					
	Frontal Cortex					
	Parietal Cortex					
	Temporal Cortex					
	Leptomeninges					
	Choroid Plexuses					

References

1. Ellul MA, Benjamin L, Singh B, et al (2020) Neurological associations of COVID-19. Lancet Neurol. 19:767–783, doi:10.1016/s1474-4422(20)30221-0.
2. Helms J, Kremer S, Merdji H, et al. (2020) Neurologic Features in Severe SARS-CoV-2 Infection. N. Engl. J. Med. 382:2268–2270, doi:10.1056/nejmc2008597.
3. Huang C, Huang L, Wang Y, et al. (2021) 6-month consequences of COVID-19 in paients discharged from hospital: a cohort study. Lancet 397:220-232.
4. Iadecola C, Anrather J, Kamel H (2020) Effects of COVID-19 on the Nervous System. Cell 183:16–27, doi:10.1016/j.cell.2020.08.028.
5. Mao L, Jin H, Wang M, et al. (2020) Neurologic Manifestations of Hospitalized Patients with Coronavirus Disease 2019 in Wuhan, China. JAMA Neurol. 77:683, doi:10.1001/jamaneurol.2020.1127.
6. Puelles VG, Lütgehetmann M, Lindenmeyer MT, et al. (2020) Multiorgan and Renal Tropism of SARS-CoV-2. N. Engl. J. Med. 383:590–592, doi:10.1056/nejmc2011400.

7. Jacob F, Pather SR, Huang WK, Zhang F, et al. (2020) Human Pluripotent Stem Cell-Derived Neural Cells and Brain Organoids Reveal SARS-CoV-2 Neurotropism Predominates in Choroid Plexus Epithelium. Cell Stem Cell. 27:937-950. doi: 10.1016/j.stem.2020.09.016.
8. Matschke J, Lütgehetmann M, Hagel C, Sperhake JP, Schröder AS, Edler C, Mushumba H, Fitzek A, Allweiss L, Dandri M, Dottermusch M, Heinemann A, Pfefferle S, Schwabenland M, Sumner Magruder D, Bonn S, Prinz M, Gerloff C, Püschel K, Krasemann S, Aepfelbacher M, Glatzel M (2020) Neuropathology of patients with COVID-19 in Germany: a post-mortem case series. Lancet Neurol. 19:919-929. doi: 10.1016/S1474-4422(20)30308-2.
9. Meinhardt J, Radke J, Dittmayer C, Franz J, Thomas C, Mothes R, Laue M, Schneider J, Brünink S, Greuel S, Lehmann M, Hassan O, Aschman T, Schumann E, Chua RL, Conrad C, Eils R, Stenzel W, Windgassen M, Rößler L, Goebel HH, Gelderblom HR, Martin H, Nitsche A, Schulz-Schaeffer WJ, Hakroush S, Winkler MS, Tampe B, Scheibe F, Körtvélyessy P, Reinhold D, Siegmund B, Kühl AA, Elezkurtaj S, Horst D, Oesterhelweg L, Tsokos M, Ingold-Heppner B, Stadelmann C, Drosten C, Corman VM, Radbruch H, Heppner FL (2021) Olfactory transmucosal SARS-CoV-2 invasion as a port of central nervous system entry in individuals with COVID-19. Nat Neurosci. 24:168-175. doi: 10.1038/s41593-020-00758-5.
10. Porzionato A, Emmi A, Contran M, Stocco E, Riccetti S, Sinigaglia A, Macchi V, Barzon L, De Caro R (2021) The Carotid Body in COVID-19: histopathological and virological analyses of an autopsy case series. Front. Immunn. doi:10.3389/fimmu.2021.736529
11. Solomon IH, Normandin E, Bhattacharyya S, Mukerji SS, Keller K, Ali AS, Adams G, Hornick JL, Padera RF Jr, Sabeti P (2020) Neuropathological Features of Covid-19. N Engl J Med. 383:989-992. doi: 10.1056/NEJMc2019373.
12. Trevisan M, Riccetti S, Sinigaglia A, Barzon L (2021) SARS-CoV-2 Infection and Disease Modelling Using Stem Cell Technology and Organoids. Int J Mol Sci 22:2356.
13. Bauer L, Lendemeijer B, Leijten L, Embregts CWE, Rockx B, Kushner SA, de Vrij FMS, van Riel D (2021) Replication Kinetics, Cell Tropism, and Associated Immune Responses in SARS-CoV-2- and H5N1 Virus-Infected Human Induced Pluripotent Stem Cell-Derived Neural Models. mSphere 6:e0027021. doi: 10.1128/mSphere.00270-21.
14. Pellegrini L, Albecka A, Mallery DL, Kellner MJ, Paul D, Carter AP, James LC, Lancaster MA (2020) SARS-CoV-2 Infects the Brain Choroid Plexus and Disrupts the Blood-CSF Barrier in Human Brain Organoids. Cell Stem Cell. 27:951-961.e5. doi: 10.1016/j.stem.2020.10.001.
15. Song E, Zhang C, Israelow B, Lu-Culligan A, Prado AV, Skriabine S, Lu P, et al. (2021) Neuroinvasion of SARS-CoV-2 in human and mouse brain. J Exp Med. 218:e20202135. doi: 10.1084/jem.20202135.
16. Zheng J, Wong LR, Li K, Verma AK, Ortiz ME, Wohlford-Lenane C, Leidinger MR, Knudson CM, Meyerholz DK, McCray PB Jr, Perlman S (2021) COVID-19 treatments and pathogenesis including anosmia in K18-hACE2 mice. Nature. 589:603-607. doi: 10.1038/s41586-020-2943-z.
17. Desforges M, Le Coupanec A, Stodola JK, Meessen-Pinard M, Talbot PJ (2014) Human coronaviruses: viral and cellular factors involved in neuroinvasiveness and neuropathogenesis. Virus Res. 194:145-58. doi: 10.1016/j.virusres.2014.09.011.
18. Schwabenland M, Salié H, Tanevski J, Killmer S, Lago MS, Schlaak AE, Mayer L, Matschke J, Püschel K, Fitzek A, Ondruschka B, Mei HE, Boettler T, Neumann-Haefelin C, Hofmann M, Breithaupt A, Genc N, Stadelmann C, Saez-Rodriguez J, Bronsert P, Knobeloch KP, Blank T, Thimme R, Glatzel M, Prinz M, Bengsch B (2021) Deep spatial profiling of human COVID-19 brains reveals neuroinflammation with distinct microanatomical microglia-T-cell interactions. Immunity. 54:1594-1610.e11. doi: 10.1016/j.immuni.2021.06.002.
19. Lee MH, Perl DP, Nair G, Li W, Maric D, Murray H, Dodd SJ, Koretsky AP, Watts JA, Cheung V, Masliah E, Horkayne-Szakaly I, Jones R, Stram MN, Moncur J, Hefti M, Folkerth RD, Nath A (2021) Microvascular Injury in the Brains of Patients with Covid-19. N Engl J Med. 384:481-483. doi: 10.1056/NEJMc2033369.
20. Yang AC, Kern F, Losada PM, Agam MR, Maat CA, Schmartz GP, et al. (2021) Dysregulation of brain and choroid plexus cell types in severe COVID-19. Nature. 595:565-571. doi: 10.1038/s41586-021-03710-0.
21. Schurink B, Roos E, Radonic T, et al. (2020) Viral presence and immunopathology in patients with lethal COVID-19: a prospective autopsy cohort. Lancet Microbe. 1:e290-e299
22. Barton LM, Duval EJ, Stroberg E, Ghosh S, Mukhopadhyay S (2020) COVID-19 Autopsies, Oklahoma, USA. Am J Clin Pathol 153:725-733. doi: 10.1093/ajcp/aqaa062.
23. Reichard RR, Kashani KB, Boire NA, Constantopoulos E, Guo Y, Lucchinetti CF (2020) Neuropathology of COVID-19: a spectrum of vascular and acute disseminated encephalomyelitis (ADEM)-like pathology. Acta Neuropathol. 140:1-6. doi: 10.1007/s00401-020-02166-2.
24. Schaller T, Hirschbühl K, Burkhardt K, Braun G, Trepel M, Märkl B, Claus R (2020) Postmortem Examination of Patients With COVID-19. JAMA 323:2518-2520. doi: 10.1001/jama.2020.8907.
25. Lavezzo E, Franchin E, Ciavarella C, Cuomo-Dannenburg G, Barzon L, et al. (2020) Suppression of a SARS-CoV-2 outbreak in the Italian municipality of Vo'. Nature. 584:425-429. doi: 10.1038/s41586-020-2488-1.
26. Mai, J. K., and Paxinos, G. (2012). *The Human Nervous System*, 3rd Edn. Amsterdam: Elsevier.

27. Basso C, Leone O, Rizzo S, De Gaspari M, van der Wal AC, Aubry MC, Bois MC, Lin PT, Maleszewski JJ, Stone JR. Pathological features of COVID-19-associated myocardial injury: a multicentre cardiovascular pathology study. Eur Heart J. 2020 Oct 14;41(39):3827-3835. doi: 10.1093/eurheartj/ehaa664.
28. Porzionato A, Stocco E, Emmi A, Contran M, Macchi V, Riccetti S, Sinigaglia A, Barzon L, De Caro R (2021) Hypopharyngeal Ulcers in COVID-19: Histopathological and Virological Analyses - A Case Report. Front Immunol. 12:676828. doi: 10.3389/fimmu.2021.676828.
29. Li YC, Bai WZ, Hashikawa T (2020) The neuroinvasive potential of SARS-CoV2 may play a role in the respiratory failure of COVID-19 patients. J Med Virol.92:552-555. doi: 10.1002/jmv.25728.
30. Porzionato A, Emmi A, Barbon S, Boscolo-Berto R, Stecco C, Stocco E, Macchi V, De Caro R (2020) Sympathetic activation: a potential link between comorbidities and COVID-19. FEBS J 287:3681-3688. doi: 10.1111/febs.15481.
31. Porzionato A, Emmi A, Stocco E, Barbon S, Boscolo-Berto R, Macchi V, De Caro R (2020) The potential role of the carotid body in COVID-19. Am J Physiol Lung Cell Mol Physiol. 319:L620-L626. doi: 10.1152/ajplung.00309.2020.
32. Iturriaga R & Castillo-Galán S (2019) Potential contribution of carotid body-induced sympathetic and renin-angiotensin system overflow to pulmonary hypertension in intermittent hypoxia. Curr Hypertens Rep 21, 89.
33. Deigendesch N, Sironi L, Kutza M, Wischnewski S, Fuchs V, Hench J, Frank A, Nienhold R, Mertz KD, Cathomas G, Matter MS, Siegemund M, Tolnay M, Schirmer L, Pröbstel AK, Tzankov A, Frank S. Correlates of critical illness-related encephalopathy predominate postmortem COVID-19 neuropathology. Acta Neuropathol. 2020 140:583-586. doi: 10.1007/s00401-020-02213-y.
34. Emmi A, Antonini A, Macchi V, Porzionato A, De Caro R (2020) Anatomy and Connectivity of the Subthalamic Nucleus in Humans and Non-human Primates. Front Neuroanat. 2020 14:13. doi: 10.3389/fnana.2020.00013.
35. Emmi A, Porzionato A, Contran M, De Rose E, Macchi V, De Caro R (2021) 3D Reconstruction of the Morpho-Functional Topography of the Human Vagal Trigone. Front Neuroanat. 15:663399. doi: 10.3389/fnana.2021.663399.

Figures

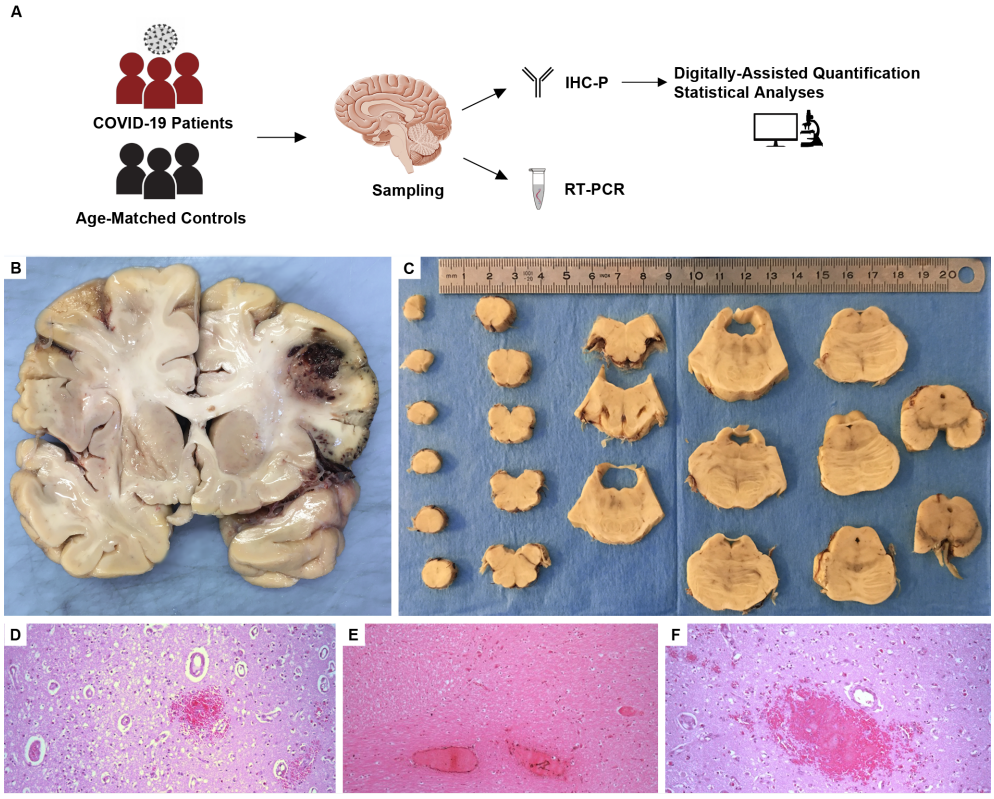

Figure 1

A) Study Workflow. Brain sections of multiple sites were sampled from 24 COVID-19 patients and 10 Age-matched controls with comparable medical conditions. B) Coronal brain section of Subject #11 revealing extensive haemorragic injury in the territory of the middle cerebral artery. C) Sampling procedure of the brainstem through axial sections passing perpendicularly to the floor of the fourth ventricle. D) Subject #11, Subcortical white matter; marked endothelitis of small subcortical vessels associated to perivascular extravasation and moderate oedema. E) Small vessel platelet thromboses at the level of the pons in Subject #19; F) Perivascular hemorrhage in a thrombotic vessel at the level of the cortical gray matter in Subject #20. G-I) Platelet microthrombi at the level of the pons and cerebral cortex, CD61 immunohistochemistry. Scale Bars: 100µm (D-G); 50µm (H-I).

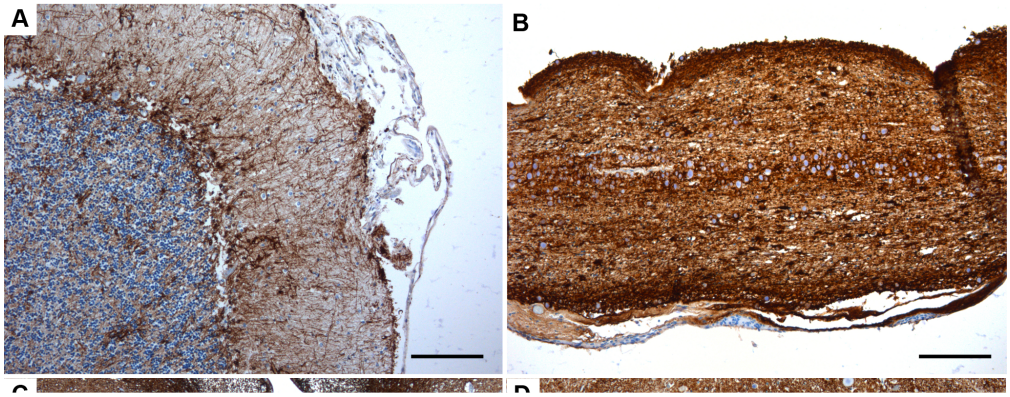

Figure 2

GFAP Immunohistochemistry. A) Reactive Bergmann Glia at the level of the cerebellar cortex in Subject #2. B) Marked astrogliosis with numerous corpora amylacea could be appreciated in this sagittal section of the olfactory tract. C) Reactive astrocytosis was marked within the subependymal regions of the medullary tegmentum, also displaying numerous reactive astrocytes within the hypoglossal nucleus. D) Reactive Astrocytosis surrounding the central canal of the lower medulla. E) Reactive astrocytes within the basilary pons in Subject #3. F) Reactive astrocytes at the level of the substantia nigra in the mesencephalon. Scale Bars: 200µm (C); 100µm (A,B,D,E); 50µm (F).

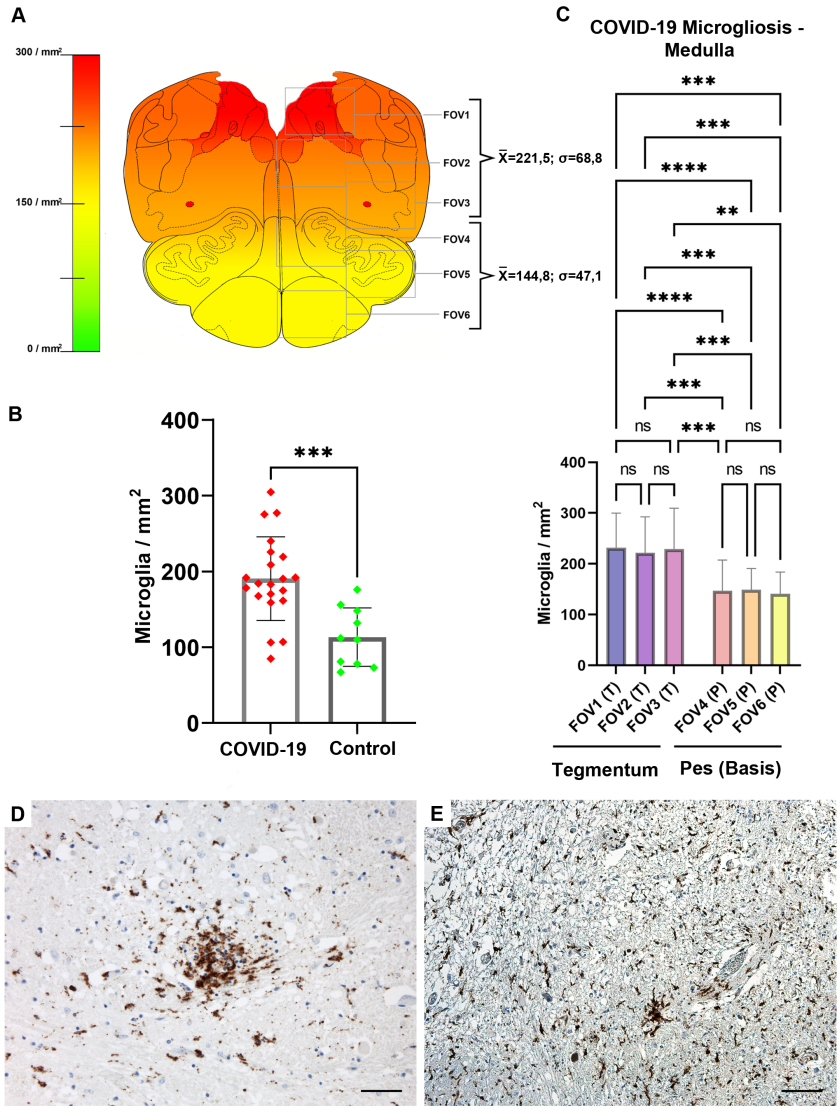

Figure 3

A) Anatomical heatmap of activated microglia within the medulla oblongata. B) Welch's corrected T-Test plot of manually-counted activated microglia within the medulla oblongata in COVID-19 subjects (red) vs controls (green), revealing statistically significant differences ($p<0.001$) between groups. C) one-way ANOVA of activated microglial densities per Field of View (FOV) reveals statistically significant differences between FOVs of the Tegmentum (T; FOV1-3) when compared to FOVs of the Pes (P; FOV4-6) (. D) Microglial nodule in the context of the medullary reticular formation, CD68 immunohistochemistry. E) Activated microglia at the level of the Solitary Tract Nucleus and Area Postrema with a small microglial star, HLA-DR immunohistochemistry. Scale Bars: 100µm.

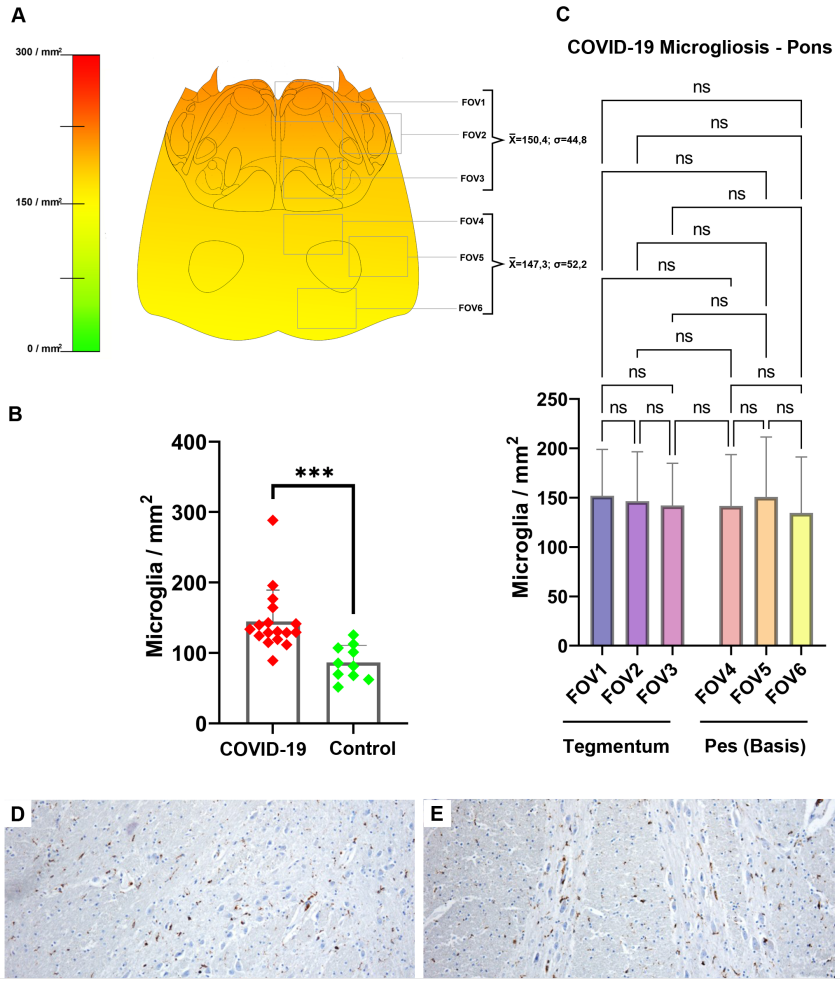

Figure 4

A) Anatomical heatmap of activated microglia within the pons. B) Welch's corrected T-Test plot of manually-counted activated microglia within the pons in COVID-19 subjects (red) vs controls (green), revealing statistically significant differences ($p<0.001$) between groups. C) one-way ANOVA of activated microglial densities per Field of View (FOV) reveals no statistically significant differences between FOVs, regardless of anatomical boundaries. D-E) Activated microglia at the level of the Basilary Nuclei of the Pons, CD68 immunohistochemistry. Scale Bars: 100µm.

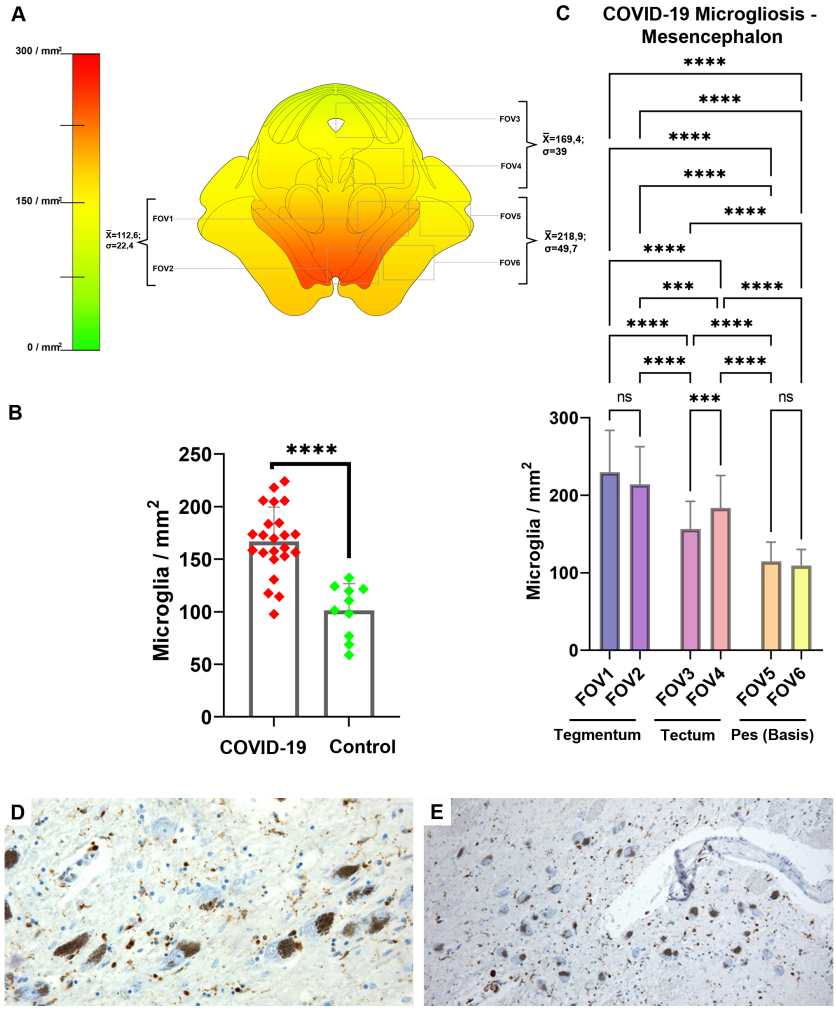

Figure 5

A) Anatomical heatmap of activated microglia within the mesencephalon. B) Welch's corrected T-Test plot of manually-counted activated microglia within the mesencephalon in COVID-19 subjects (red) vs controls (green), revealing statistically significant differences ($p<0.0001$) between groups. C) one-way ANOVA of activated microglial densities per Field of View (FOV) reveals statistically significant differences between FOVs of the Tegmentum, Tectum and Pes, with higher densities of activated microglia fund within the Tegmentum. D-E) Activated microglia at the level of the Substantia Nigra, CD68 immunohistochemistry. Scale Bars: 100µm.

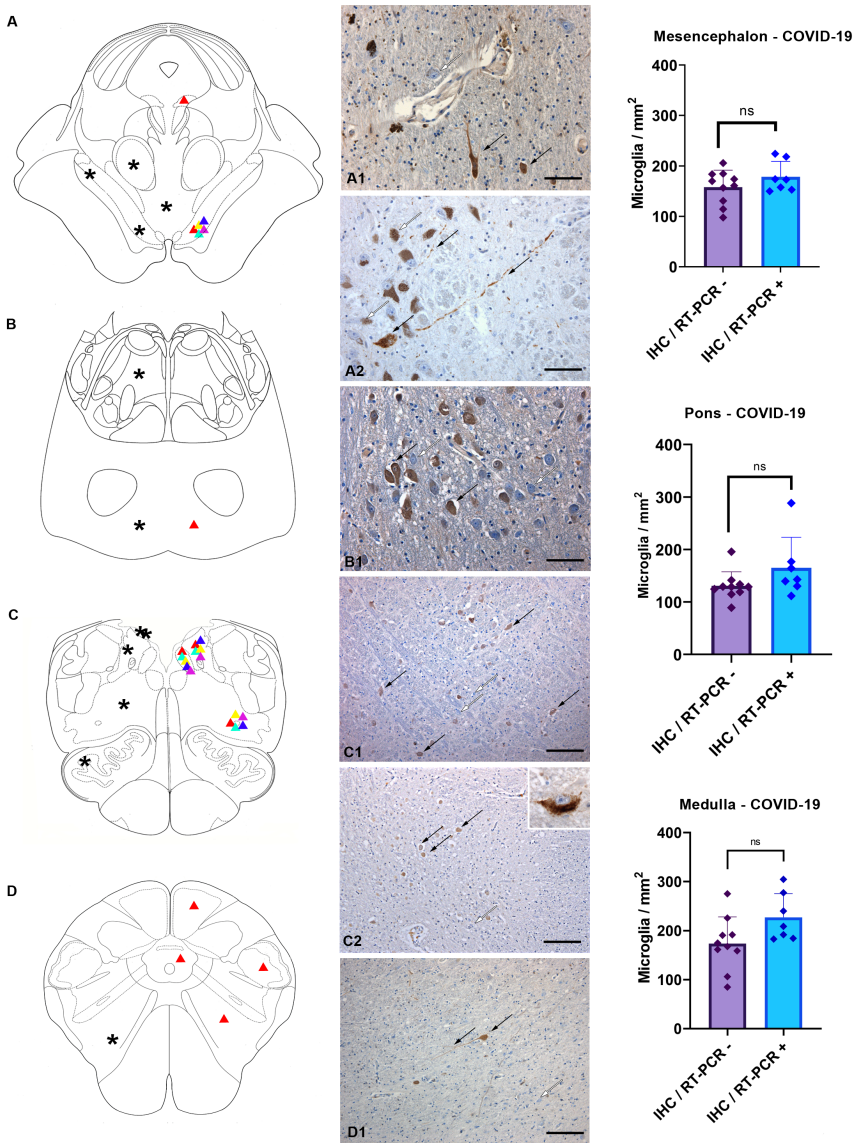

Figure 6

Topographical localization of SARS-CoV-2 Viral Protein Immunoreactivities (Triangles, Right Half) and Microglial Nodules (Asterisks, Left Half) throughout the brainstem. A) At the level of the Mesencephalon, Immunoreactivities are found mainly within the boundaries of the substantia nigra, with the exception of Subject #3, which also presented immunoreactive neurons within the Interstitial Nucleus of Cajal; Microglial stars were confined mainly within the boundaries of the tegmentum, and were not detected neither within the pes nor the tectum. A1) SARS-CoV-2 Spike Protein IHC at the level of the Substantia Nigra reveals several immunoreactive neurons with well-marked processes (black arrows); negative neurons can also be found nearby (white arrows). A2) SARS-CoV-2 Nucleocapsid Protein IHC reveals sparse immunoreactive neurons and axons throughout the substantia nigra. B) At the level of the Pons, Subject #3 presented numerous immunoreactive neurons within the basilary nuclei, while microglial stars were found both within the basis, as well as the dorsal pons in proximity to the facial nucleus. B1) SARS-CoV-2 Spike Protein IHC at the level of the pons in Subject #3, displaying numerous immunoreactive neurons (black arrows) within the basilary nuclei of the pons; non-reactive cells can also be appreciated (white arrows) C) At the level of the Upper Medulla Oblongata, Immunoreactivities were found at the level of the Dorsal Motor Nucleus of the Vagus, Solitary Tract Nucleus and Nucleus Ambiguus; Microglial stars were prominent within the Vagal Trigone and Area Postrema, but were also found within the reticular formation and the inferior olivary complex. C1-2) SARS-CoV-2 Spike Protein IHC at the level of the solitary tract nucleus and nucleus ambiguus; immunoreactive neurons can be seen within the anatomical boundaries of these nuclei (black arrows), along with non-reactive cells (white arrows). Magnification of a single reactive neuron within the Solitary Tract Nucleus, Spike Protein immunohistochemistry. D) At the level of the Lower Medulla Oblongata, Immunoreactivities were found at the level of the Spinal Trigeminal Nucleus and medullary reticular formation. Microglial stars were found within the medullary reticular formation. D1) SARS-CoV-2 Spike Protein IHC at the level of the medullary reticular formation in the lower medulla (black arrows); non-reactive cells are indicated with a white arrow. Scale Bars: 100µm (C1,C2,D1); 50µm (A1,A2,B1).

Supplementary Files

This is a list of supplementary files associated with this preprint. Click to download.

- SupplementaryTable1.docx
- Supplementaryfigure1.tif
- SupplementaryFigure2.tif
- nrreportingsummaryNCOMMS2144215.pdf